ISBN: 978-981-18-5852-9
WCSE 2022 Spring Event: 2022 9th International Conference on Industrial Engineering and Applications
doi: 10.18178/wcse.2022.04.016

Investigation of Module-Level Hot-Spot Suppression During Power Generation in Photovoltaic Systems

Kazutaka Itako [1], Zhangyin Hong [1], Tsugutomo Kudoh [1] and Keishin Koh [1]

[1] Kanagawa Institute of Technology Department of Electrical and Electronic Engineering

Abstract. This study proposes an adaptive control system for achieving module-level hot-spot detection and suppression during power generation in photovoltaic (PV) systems. Hot-spots form at shaded locations where low-resistance defects under reverse bias are non-uniformly heated within a short period of time. In order to detect malfunctioning modules, a scan-based distributed control system is employed in this study. The behavior of each module in a PV array is monitored via a periodic scan. In addition, alternative control patterns for hot-spot suppression and normal situations are proposed. This control system was validated by experiments using a laboratory prototype. The results indicate that the module-level hot-spot suppression is robust, allowing safe operation of the PV generation system.

Keywords: Distributed control strategy, hot-spot phenomenon, low-resistance defects, photovoltaic (PV) generation system, safe operation.

1. Introduction

The real-time monitoring and fault diagnosis of photovoltaic (PV) generation systems has attracted extensive research attention in recent decades [1]-[3]. Particularly, in the term of hot-spot phenomenon, it has been reported that compared with classical hot-spots [4]-[8], those resulting from low-resistance defects (LRDs) in c-silicon PV cells with high temperatures may lead to more severe damage to the system in the absence of alarms or protection [9]-[15].

Our prior work [15] analysed the fundamental mechanism of these hot-spots with a series of schematic diagrams and simulations. Analytical results have shown that extra current paths are created by LRDs under reverse bias in partial shading conditions [16]-[17]. A high and prolonged reverse current can easily flow through these paths, continuously heating the defective regions when a maximum power point tracking (MPPT) controller is used.

Based on previous studies, for the purpose of locating malfunctioning modules during power generation and reducing the undesired safe-operation-induced power loss in a full string, the present study proposes a systematic hybrid control system with a distributed structure, basically, a DC-DC converter (Unit) is installed for each module. Besides, with the distributed structure, the module-level MPPT control can be also executed. Therefore, the key features of this technique are shown as follows:

1) It provides module-level hot-spot detection and suppression.

2) It allows independent MPPT operation of each module to make the PV string active when in absence of hot-spot.

2. Principle of hot-spot suppression

In the LRD-induced thermal power distributions obtained from simulations [15], three operating modes, namely I, II, and III in Fig. 1, can be distinguished based on the magnitude of current from the open circuit to the short circuit. Especially, X represents shadow ratio for one solar cell, and if a cell is shaded by this shadow, the maximum photo current which can be generated by this cell turns to be $(1\text{-}X)I_{SC}$. In mode I, the current is less than the maximum photo current, ensuring that thermal power is zero because the defective module operates at forward bias. In mode II, the derivative of the current with respect to voltage is nearly constant and equal to the conductance at the equivalent resistance. In this mode, the current is greater than above-mentioned photo current, and the exceeding part of the photo current starts flowing through the LRDs-

induced resistance at defective regions, resulting in nonzero thermal power. Finally, in mode III, the bypass diode turns on. Even if the bypass diode functions in current diversion, allowing current, I_{PV1}, still smoothly flow through the defective regions. In this case, the defective module undergoes the maximum reverse bias, and will be heated up significantly.

Based on these features, a hybrid control method involving a periodic scanning process was employed. In this method, the transient scan process started from open circuit (OC) to short circuit (SC) with a continuous declined unit voltage, therefore, the real-time I-V curve can be acquired according to the characterization of the solar module. During scan process, the derivative of the current with respect to voltage can also be calculated simultaneously. Following this, if the calculated value is nonzero constant in mode II, it is confirmed that the LRDs-induced hot-spots exist firmly. Moreover, once such hot-spots occur in defective regions, a safe control was proposed to suppress these hot-spots in a PV string by shifting the operation voltage from maximum power point voltage, V_{MPP}, to safe operation point voltage, V_{SOV}, lying between mode I and II.

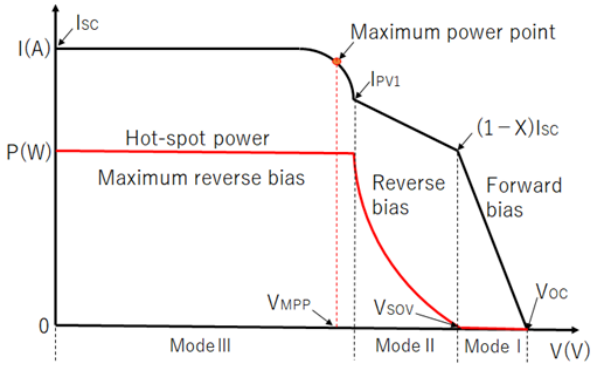

Fig. 1: Schematic diagram of safe operation for the suppression of LRD-induced hot-spots.

3. Proposed control system

3.1. Configurations

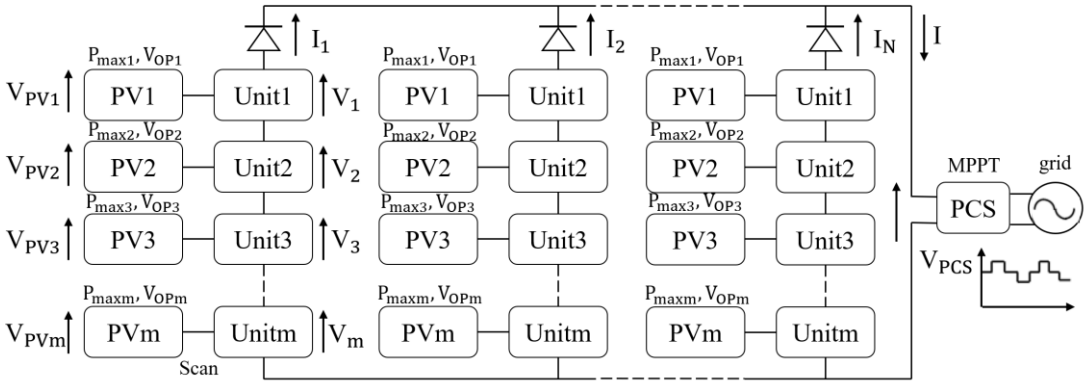

Fig. 2: Construction of actual-scale proposed PV system.

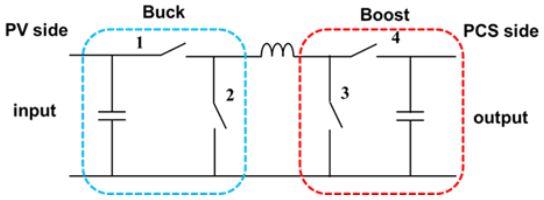

Fig. 3: Buck-Boost DC-DC Converter (Unit).

In this section, the proposed systematic control strategy, shown in Fig. 2, is described. Fig.3 shows the buck-boost DC-DC converter used in the unit. Assuming that a PV string consists of any number of modules (m modules), two cases are considered: (i) malfunctioning modules with hot-spots and (ii) all modules without hot-spots. The behavior of each module is monitored in real time by scanning the signals provided by the digital signal processor. Accordingly, alternative control patterns are proposed after hot-spot detection.

It can be observed that one is safe control for hot-spots, and the other is transfer control for those modules without hot-spot (including unidentified malfunctioning modules). The generalized control strategy is demonstrated with some formulations.

3.2. Control Strategy

a) Safe Control for Hot-Spots

Since hot-spots can form in any malfunctioning module, both the safe operating voltage, $V_{SOV}(i)$, and power, $P_{SOV}(i)$, are kept at safe levels. As mentioned in Section I, during previous trials, the operating point was controlled from the MPP to the safe operating point, $V_{SOV}(i)$, for suppressing the nonzero thermal power that results from pronounced hot-spots. In this scenario, the reference voltage for hot-spots can be expressed as:

$$V_{ref}(i) = V_{SOV}(i) \tag{1}$$

In this control pattern, the operating voltage of each malfunctioning module is simply its own, V_{SOV}. Therefore, these modules can work at their respective safe state.

b) Transfer Control for Normal cases (Without Hot-Spot)

In the absence of hot-spots, transfer control is proposed for all modules (including malfunctioning modules). Unlike safe control, in this control pattern, the main objective is to guarantee that such modules work at their own MPP for energy harvesting using the transfer coefficient refreshed during scanning process. Where, $V_{out}(i)$ is matched output voltage of each converter in real time. The value of each output is:

$$V_{ouy}(i) \approx \frac{P_i \cdot V_{pcst}}{\sum_{i=1}^{m} P_i} \tag{2}$$

Where, V_{pcst} is the real-time operating voltage at PCS side. Due to the series structure, the output voltage of each converter is approximately determined by the magnitude of solar power generated by its own.

The reference voltage for each module without hot-spot can be simplified as follows:

$$V_{ref}(i) = \frac{1}{\gamma_i} \cdot V_{out}(i) \approx \frac{V_{mpp}(i) \cdot \sum_{i=1}^{m} P_i}{P_{max}(i) \cdot V_{pcs0}} \cdot \frac{P_{max}(i) \cdot V_{pcst}}{\sum_{i=1}^{m} P_i} = \frac{V_{pcst}}{V_{pcs0}} \cdot V_{mpp}(i) \tag{3}$$

Where, $V_{mpp}(i)$ is MPP (optimal) voltage of each module acquired from scan in normal cases. Note that unlike safe control for hot-spots, the value of transfer coefficient is also used for calculation in this pattern. Moreover, due to MPPT at the PCS side, V_{pcst} is always approaching the set constant, V_{pcs0}, allowing the reference voltage of each module to approach its MPP voltage refreshed after scan. That is, the optimal voltage can be regulated appropriately from the PCS side to each module. This directly indicates that the transfer control ensures each module operate at their own MPP when there is no hot-spot even sharing one MPPT controller with constant bus voltage at PCS side.

4. Experimental results

In order to assess the practical feasibility of this proposed control system, experimental verification obtained using a 212W laboratory prototype are given in this section.

4.1. Specifications of the PV Modules

As an example of hybrid use of PV modules, the PV array consists of two 56W and two 50W modules.

Table 1 shows the specifications of the modules used. Fig. 4 shows the internal structure of the PV module. The cell group consists of two clusters with two bypass diodes.

Table 1: Specifications of PV Modules (Under Nominal Conditions)

Description	SYMBOL	Value
Maximum power	P_{MAX}	50 W/56W
Open-circuit voltage	V_{OC}	20.5 V/21.1V
Short-circuit current	I_{SC}	3.47 A/3.47A
Maximum power point voltage	V_{MPP}	16.4 V/17.2V
Maximum power point current	I_{MPP}	3.05 A/3.26A

Note: nominal conditions: irradiance is 1000W/m^2, the temperature of solar cell is 25°C.

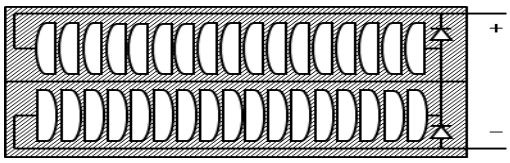

Fig. 4: Internal structure of PV module.

4.2. Environmental conditions

Table 2 shows the environmental conditions during the experiment.

Table 2: Environmental Conditions

Description	Value
Irradiance	600～700 W/m2
Temperature of solar cell	23.0 °C

4.3. Experimental configuration

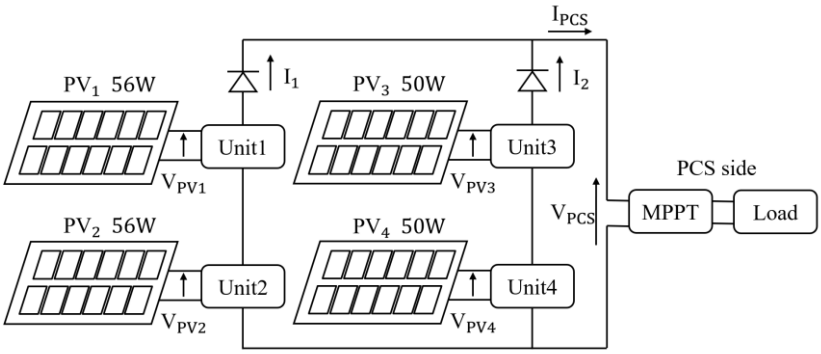

Fig. 5: Simplified experimental configuration.

Figure 5 shows the simplified experimental configuration used to validate adaptive operation for various situations. In this configuration, PV4 is known as malfunctioning module with low-resistance defects, while PV1, PV2 and PV3 are normal modules. Two DC-DC converters controlled by DSP (digital signal processor) were connected in series with the same MPPT controller at PCS side. Here, MPPT operation provided by PCS side was implemented with the conventional P&O approach. In addition, the theoretically optimal operating voltage, V_{pcs0}, at the PCS side used for calculation was initially set as 36 V. It is worth noting that this value is not fixed and determined by user's requests. For example, in our research, the DC-DC converters are expected to work at boost mode for high output voltage on the occasion when in absence of a shadow. Since the total value of MPP voltages at nominal conditions (34.4V/32.8V) is always less than this set value (36V), such that both of converters can work at boost mode to a certain extent.

Moreover, the general procedure is as follows: the experimental trials started during power generation when there was no shadow to verify the MPPT operation, we called it pattern A. Next, following step ①, in step ②, we added a partial shadow at the defective cell to confirm the hot-spot detection and suppression (pattern B). The related results of these operations are given in next section in detail. Fig.6 shows the PV array used in the experiment.

Fig.6 PV array used in the experiment.

4.4. Results

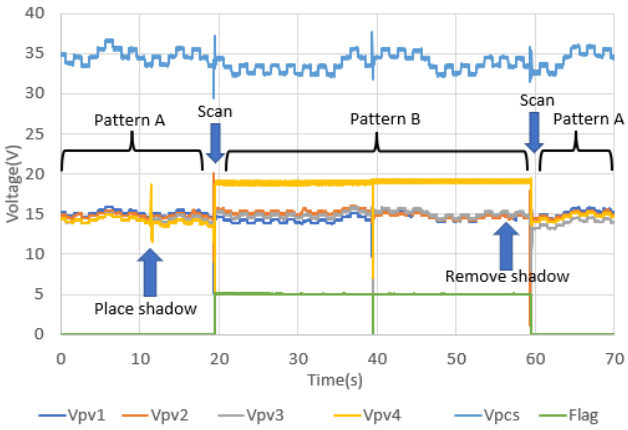

Fig. 7: Experimental waveforms before and after placing and removing shadow.

The waveform of experiment is shown in Figure 7. 90 percent of the defective cell area in PV4 was shaded in this experiment. The system was operated without shading at the beginning.

So, we can see that in the first 20 seconds of the waveform, the system is running MPPT control in each PV module. Although we placed the shadow on the defective cell before the time reached 20 seconds, the system did not respond because it was not yet time to scan. At 20 seconds, the system reached the set scan time (once every 20s) and performed a scan of hotspot. After 30ms of I-V characteristic scanning, the system detected the presence of hotspot. To indicate the system`s judgment on the presence or absence of hotspots, a 5V flag signal is output when hotspot is detected. And to avoid heat generation, the voltage of the module where the hot spot is located is controlled to the V_{SOV} mentioned in Figure 1. The V_{SOV} in this experiment was 19V. As we can see from the waveform graph in Figure 7, the system completed the detection of hot spots and completed the voltage control as required. And it did not affect other modules to generate electricity. After the scan after removing the shadows, the system also detects the removal of the shadows, and the defective module is back into MPPT control.

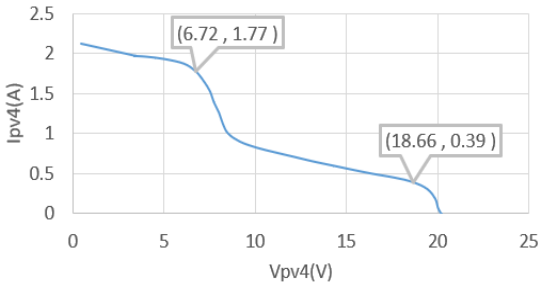

Fig. 8: I-V characteristics of PV module after shading

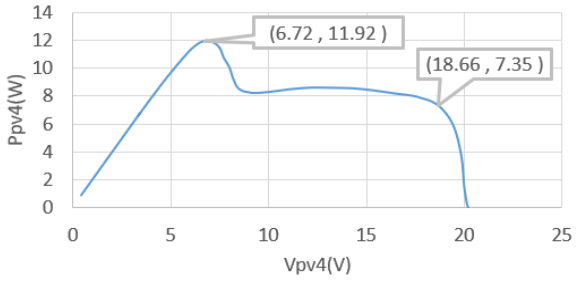

Fig. 9: P-V characteristics of PV module after shading

The I-V characteristics of module with shaded defective cell are shown in Figure 8. And the P-V characteristics of the module with shaded defective cell are shown in Figure 9. It can be seen that the maximum power point of the module is 6.7V when the shadow shades 90 percent of the defective cell area. If operating MPPT on the shaded module at this time, the module will operate in mode III as shown in Figure

1. The reverse current through the PN junction of the defective cell reaches its maximum and will generate a lot of heat.

The voltage in the experiment was controlled to 19V, which is the highest power point in mode I. This is the highest power generation point without heat generation.

To test the effect of heat suppression more directly, two experiments were conducted with and without heat suppression.

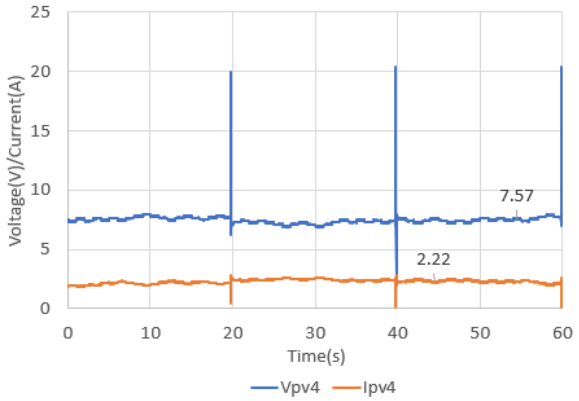

Fig. 10: Voltage and current of defective modules without suppression of heat generation.

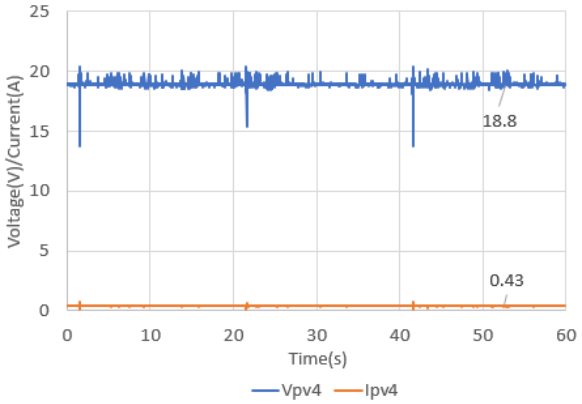

Fig. 11: Voltage and current of defective modules with suppression of heat generation.

The voltages and currents of the defective modules in both cases are shown in Figure 10 and Figure 11. Without hot spot suppression, the MPPT control makes the module operate at about 7.5V. The current is greater than 2A. In comparison, with heat suppression control, the voltage is about 18.8V and the current is only 0.43A. The temperature of the defective cell after being kept in these two states for 10 minutes is shown in Figure 12 and Figure 13.

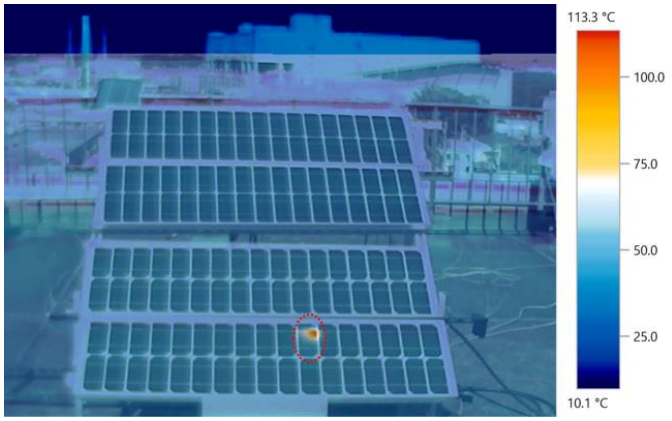

Fig. 12: Thermal image of non-running heat suppression

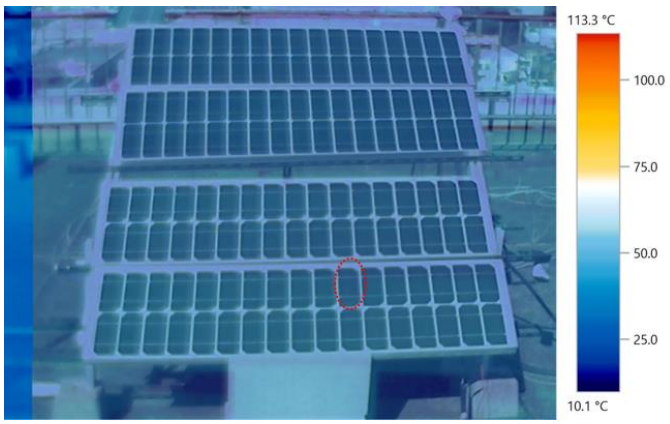

Fig. 13: Thermal image of running heat suppression

The shaded defective cell is in the second row counting from bottom to top, seventh column from right to left. The defective area is pointed out by sp1.

The temperature of the defective cell rose up to 113.3°C after it was shaded for ten minutes without heat suppression. This is 80°C higher than the temperature of the surrounding cells. While the temperature of same cell was only 30°C after shaded for ten minutes with heat suppression. This is the same as the temperature of the surrounding cells.

5. Conclusion

This study proposed a novel control system for module-level hot-spot detection and suppression. In this system, a transient scanning process provided by DC-DC converters is used to monitor the behaviour of each PV module in real time. In addition, a corresponding systematic control strategy is proposed to achieve adaptive module-level operation for various situations. The proposed system was validated by a series of experimental trials using a laboratory prototype. The results confirmed that independent hot-spot suppression and module-level MPPT operation can be accurately achieved. The proposed control system allows the PV generation system to operate safely while reducing the safe-operation-induced power loss to a low level by compared with the prior method.

6. References

[1] K. A. Saleh, et al., “Voltage-Based Protection Scheme for Faults Within Utility-Scale Photovoltaic Arrays,” IEEE Trans. Smart Grid, vol. 9, no. 5, Sept. 2018.

[2] R. Hariharan et al., “A Method to Detect Photovoltaic Array Faults and Partial Shading in PV Systems,” IEEE J. Photovolt. vol. 6, no.5, pp. 1278–1285, Sept. 2016.

[3] F. Blaabjerg et al., “Distributed Power-Generation Systems and Protection,” Proc. IEEE, vol. 105, no.7, pp. 1311-1331, Jul. 2017.

[4] T. Ghanbari, “Permanent partial shading detection for protection of photovoltaic panels against hot spotting,” IET Renew. Power Gener., vol.11, no.1, pp. 123-131, Nov. 2017.

[5] J. Poon, et al., “Photovoltaic condition monitoring using real-time adaptive parameter identification,” in Proc. IEEE Energy Convs. Congr. and Expo., 2017, pp. 1119-1124.

[6] D. Rossi, M. Omana, D. Giaffreda, and C. Metra, “Modeling and detection of hotspot in shaded photovoltaic cells,” IEEE Trans. VLSI Syst., vol. 23, no. 6, pp. 1031-1039, Jun. 2015.

[7] M. Dhimish, V. Holmes, P. Mather, and M. Sibley, “Novel hot spot mitigation technique to enhance photovoltaic solar panels output power performance,” Solar Energy, vol. 179, pp. 72-79, Jun. 2018. [Online]. Available: https:// doi.org/10.1016/j.solmat.2018.02.019.

[8] M. Simon, and E. L. Meyer, “Detection and analysis of hot-spot forma-tion in solar cells,” Solar Energy, vol. 94, pp. 106-113, Feb. 2010. [Online]. Available: https:// doi.org/10.1016/j.solmat.2009.09.016.

[9] K. Itako, and T. Kudoh, “Study on Hotspot of a Single-crystal Photo-voltaic Module,” J. Institute Electri. Installation Engi. of Japan, vol. 34, no. 2, pp. 140-146, Sept. 2014.

[10] A. Bouraiou, et.al, “Experimental investigation of observed defects in crystalline silicon PV modules under outdoor hot dry climatic conditions in Algeria,” Solar Energy, vol. 159, pp. 475-487, Jan. 2018. [Online]. Available: https://doi.org/10.1016/j.solener.2017.11.018

[11] P. Guerriero, G. Cuozzo, and S. Daliento, “Health diagnostics of PV panels by means of single cell analysis of thermographic images,” in Proc. 16th IEEE Int. Conf. Environ. and Electri. Engi., 2016, pp. 1-6.

[12] J. Gallon, G. S. Horner, J. E. Hudson, L. A. Vasilyev, and K. Lu, “PV Module Hotspot Detection,” Tau Sci. Corp., Hillsboro, OR, USA, 2015. [Online]. Available::www.nrel.gov/pv/assets/pdfs/2015 pvmrw 19 gallon.pdf

[13] K. Itako, N. Iiduka, T. Kudoh, and K. Koh, “Proposition of novel real time hot-spot detection method for PV generation system,” in Proc. IEEE Int. Conf. Smart Grid and Smart Cities, 2017, pp. 99-102.

[14] Y. D. Wang, K. Itako, T. Kudoh, K. Koh, and Q. Ge, “Voltage-Based Hot-Spot Detection Method for Photovoltaic String Using a Projector,” energies, [Online]. Available: www.mdpi.com/journal/energies, Feb. 2017.

[15] S. Yang, K. Itako, T. Kudoh, K. Koh, and Q. Ge, “Monitoring and Suppression of the Typical Hot-Spot Phenomenon Resulting from Low-Resistance Defects in a PV String,” IEEE J. Photovolt., vol. 8, no. 6, pp. 1809-1817, Nov. 2018.

[16] W. K. Loke, S. F. Yoon, S. Wicaksono, K. H. Tan, and K. L. Lew, “De fect-induced trap-assisted tunneling current in GaInNAs grown on GaAs substrate,” J. Appl. Phys., Jul. 2007. [Online]. Available: https://doi.org/ 10.1063/1.2775908.

[17] S. Steingrube, O. Breitenstein, K. Ramspeck, S. Glunz, A. Schenk, and P. P. Altermatt, “Explanation of commonly observed shunt currents in c-Si solar cells by means of recombination statistics beyond the Shockley-Read-Hall approximation,” J. Appl. Phys., May. 2011. [Online]. Available: https:// doi.org/ 10.1063/1.3607310.